A dynamic film model of the Pulsating Heat Pipe

Vadim S. Nikolayev
ESEME, Service des Basses Températures, INAC/CEA-Grenoble, France
and
ESEME, PMMH-ESPCI, 10, rue Vauquelin, 75231 Paris Cedex 5, France
Email: vadim.nikolayev@espci.fr

Abstract
This paper deals with the numerical modelling of the pulsating heat pipe (PHP) and is based on the film evaporation/condensation model recently applied to the single bubble PHP (Das et al., 2010). The described numerical code can treat the PHP of arbitrary number of bubbles and branches. Several phenomena that occur inside the PHP are taken into account: coalescence of liquid plugs, film junction or rupture, etc. The model reproduces some of the experimentally observed regimes of functioning of the PHP like chaotic or intermittent oscillations of large amplitude. Some results on the PHP heat transfer are discussed.
Keywords: oscillating, pulsating, heat pipe, simulation

1 Introduction

The pulsating (or oscillating) heat pipe (PHP) is a long capillary tube bent into many branches and partially filled with a two-phase, usually single component, working fluid [1]. The tube is simple, a wick structure is not required. The fluid spontaneously forms multiple vapor bubbles separated by liquid plugs inside the tube. Evaporation of liquid in the hot (evaporator) sections and subsequent condensation in the cold (condenser) sections creates oscillations of the bubble-plug structure. These oscillations are very important because they lead to a substantial increase of the heat transfer rate in comparison with other types of heat pipes [2]. In addition to the latent heat transfer characteristic for them, the sensible heat transfer is important in PHP. While sweeping a section belonging to evaporator, a liquid plug accumulates the heat, which is then transferred to the condenser section when the plug penetrates there.

Because of their simplicity and high performance, PHPs are often considered as highly promising. Their industrial application is however limited because their functioning is non-stationary and thus difficult to be controlled. During the last decade, researchers have extensively studied PHPs [3]. Tong et al. [4], Miyazki and Arikawa [5], Khandekar et al. [6], Xu et al. [7], Gi et al. [8] and Inoue et al. [9] have carried out flow visualization studies with several working fluids. These experiments confirmed the existence of self-sustained thermally driven oscillations in PHPs. Several experimental groups [10–14] performed experiments with different tube diameters, configurations, orientations and filling ratios and studied the thermal performance of PHPs in different conditions. However, the functioning of PHPs is not completely understood. A complicated interplay of different hydrodynamic and phase-exchange phenomena needs to be accounted for. The experimental studies of the background physical phenomena that cause the instability or are responsible for the PHP behavior are only a few [14, 15].

There are several modeling approaches available in the literature. Shafii et al. [16] initiated the modeling approaches for multi-branch PHPs. The evaporation-condensation mass exchange was accounted for with the temperature difference terms $\propto (T_{wall} - T_i)$ where T_{wall} was either T_e or T_c depending on the bubble location. The problem was solved numerically with the explicit Euler scheme. Periodical (nearly sinusoidal) oscillations appeared after a transient. Their amplitude was small: the displacement amplitude did not exceed the evaporator size. It was concluded that the heat is transferred mainly via the sensible heat transfer; the latent heat transfer was an order of value smaller. The same model has been used later by another team [17].

It is well known from the analysis of the conventional heat pipes that in reality, most of evaporation in the evaporator occurs through the liquid films that might cover only a part of the heated surface. Dobson [18, 19] introduced a lumped meniscus model where the films are considered to be of constant thickness δ_f but of varying length. Apart from the film introduction, the model was similar to [16]. Single bubble PHP with an open end was considered. The oscillations were unstable and consisted of a nearly periodical pattern which began with a strong displacement during which the meniscus penetrated into the evaporator. This initiated high frequency declining to zero oscillations around an average position situated in the condenser. Das et al. [15] attempted to reproduce the results of Dobson with his model for the same parameters. They obtained only small amplitude periodical oscillations during which the meniscus never penetrated into the evaporator. They attributed the disagreement to the poor stability of the numerical algorithm (explicit Euler) used by Dobson. The 4th order Runge-Kutta method,

well known to be stable, was used in [15]. A rigorous analytic analysis of a simplified version of the model, where the evaporation-condensation dynamics is modeled with the $(T_{wall} - T_i)$ term, has been also carried out by Das et al. An analytic expression giving the condition, under which the self-sustained oscillations appear, was obtained. It was shown that such a model leads necessarily to small amplitude oscillations.

A 2D model of the single-bubble PHP was considered by Zhang and Faghri [20]. A conceptual difference with the previous approaches concerned the vapor equation of state. Instead of the ideal gas model, the vapor was considered to be at saturation temperature T_{sat} corresponding to its pressure P. Small amplitude periodic nearly harmonic oscillations were obtained. Holley and Faghri [21] applied the same assumption to the PHP with spatially varying diameter.

Das et al. introduced the film evaporation-condensation model. The film is introduced similarly to [18,19]. The vapor mass exchange is assumed to be limited by the heat conduction in the film like in the work [20]. This leads to the mass exchange rate $\lambda_l[T_{wall} - T_{sat}(P)]/(\delta_f h_{lv})$ where $T_{sat}(P)$ is the gas-liquid interface temperature. This approach is different from all previous approaches because a strong temperature gradient is assumed to exist in the vapor so that the temperature T of its bulk is allowed to be different from $T_{sat}(P)$. The validity of this assumption is checked in [15] *a posteriori*. The simulations have shown that most of the time $T > T_{sat}(P)$. The same form of the mass exchange term has been used recently by Senjaya et al. [22]. They however did not use the variable films. The film evaporation-condensation model was validated against the single branch experiment [15]. It reproduces oscillations the amplitude of which might be larger than the size of evaporator. The purpose of the present article is to apply it to the multi-bubble PHP. The closed loop PHP will be considered. The model is however can be applied also to the unlooped PHP.

2 Problem statement

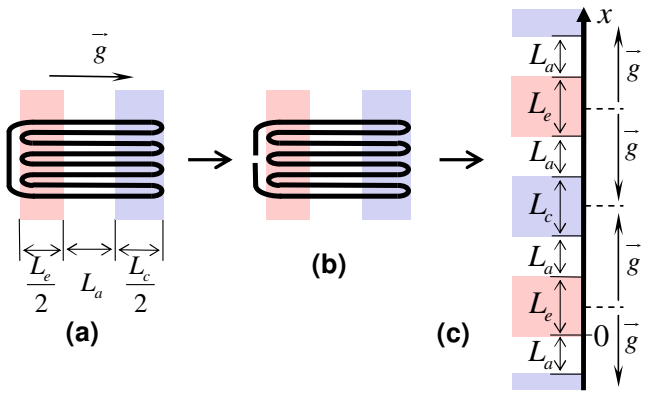

Fig. 1. (Color online) (a) Sketch of the closed loop PHP with the default gravity direction. Evaporator is to the left. (b,c) Topological transformations of the tube. (b) Unlooping. (c) Unbending and projection to the x axis. The splitting of the x axis to branches is shown.

Like in [16, 17], the PHP meandering tube is projected to a straight axis x so that it consists of periodic sequence of different domains corresponding to the PHP sections (Fig. 1). One PHP spatial "period" of the length $L_p = 2L_a + L_c + L_e$ is assumed to contain the sections in the following order: evaporator, adiabatic, condenser, adiabatic. The point $x = 0$ is assumed to coincide with the beginning of an evaporator. The PHP branch is a half of a period ($L_b = 0.5L_p$) beginning in the middle of a condenser or an evaporator. $L_t = N_p L_p$ is the total PHP length. Each bubble is identified by the index i. The neighboring from the right side liquid plug is denoted by the same index. The total number M of bubbles may change in time.

Unlike [16], the axis and the periodical pattern of sections on it are continued to infinity in both directions. At $t = 0$, the bubbles are positioned at the axis and may move at $t > 0$ along the infinite axis x as far as needed. This means that the x value itself does not have any significance; only the relative positions are meaningful; they are determined with the remainder operator defined as $y \bmod z = y - z\,\mathrm{int}(y/z) \geq 0$ where $\mathrm{int}(z)$ means the integer part of z, i.e. the largest integer smaller than z. E. g. x belongs to evaporator if $x \bmod L_p \leq L_e$. Since the PHP loop is closed, each point x is equivalent to the point $L_t + x$. Such an approach is convenient because it simplifies the management of any kind of bubble motion, in particular their unidirectional circulation. Within such a description, the coordinate X_i^l of the left meniscus of the bubble i is always smaller than that of its right meniscus X_i^r and the bubble order does not change during their motion. Note that the coordinate X_M^r of the left end of the last liquid plug is larger than that of its right end X_1^l.

The constant temperatures T_e and T_c are imposed at the inner walls of the evaporator and condenser.

2.1 Film dynamics in evaporators

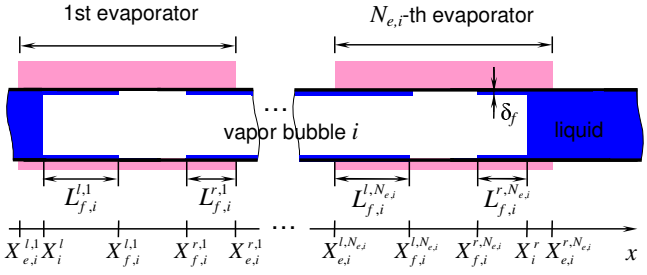

Fig. 2. (Color online) Vapor bubble i that extends over $N_{e,i}$ evaporators and the liquid films inside it.

According to the film evaporation/condensation model [15], the film length may vary because of two reasons: (i) evaporation or condensation and (ii) film deposition (Landau-Levich phenomenon) or film "eating up" during receding or advancing of the liquid meniscus, respectively. We generalize this model here to the case of multiple branches. The liquid film is assumed to always cover the inner walls

of the tube (i.e. to be continuous) in the condenser and adiabatic sections when the whole bubbles or their parts are located inside them. The film may be partially or completely evaporated in the evaporator. The films are assumed to have a homogeneous thickness δ_f in all the sections.

Let us consider the i-th bubble that may extend over several PHP bends or, equivalently, evaporators (Fig. 2). A number $N_{e,i}$ of pairs of films per bubble (left+right each) coincides with the number $\mathrm{int}(X_i^r/L_p) - \mathrm{int}[(X_i^l - L_e)/L_p]$ of evaporators to which at least a part of the bubble belongs if the latter quantity is nonzero. In the opposite case, $N_{e,i} = 1$ to describe the continuous film in the adiabatic and condenser sections. The evaporators are counted left-to-right by the index $k = 1 \ldots N_{e,i}$. The (non-negative) lengths of the left and right films of the bubble in the k-th evaporator are denoted $L_{f,i}^{l,k}$ and $L_{f,i}^{r,k}$, respectively. When the film in the evaporator is not continuous, their dynamics is described by the equations (cf. Eq. (26) of [15])

$$\dot{L}_{f,i}^{l,k} = \begin{cases} 0 & \text{if } L_{f,i}^{l,k} = 0,\ \dot{X}_i^l > 0 \text{ and} \\ & X_i^l \in k\text{-th evaporator}, \\ -\dot{m}_{fe,i}^{l,k}/(\rho_l \pi d \delta_f) & \text{if } X_i^l \notin k\text{-th evaporator}, \\ -\dot{m}_{fe,i}^{l,k}/(\rho_l \pi d \delta_f) - \dot{X}_i^l & \text{otherwise}, \end{cases} \quad (1)$$

$$\dot{L}_{f,i}^{r,k} = \begin{cases} 0 & \text{if } L_{f,i}^{r,k} = 0,\ \dot{X}_i^r < 0 \text{ and} \\ & X_i^r \in k\text{-th evaporator}, \\ -\dot{m}_{fe,i}^{r,k}/(\rho_l \pi d \delta_f) & \text{if } X_i^r \notin k\text{-th evaporator}, \\ -\dot{m}_{fe,i}^{r,k}/(\rho_l \pi d \delta_f) + \dot{X}_i^r & \text{otherwise}, \end{cases} \quad (2)$$

where dot means the time derivative. Evidently, the condition "$X_i^s \in k$-th evaporator" may be satisfied only for $k = 1$ if $s = l$ and for $k = N_{e,i}$ if $s = r$. The mass evaporation rate at k-th evaporator $\dot{m}_{fe,i}^{s,k}$ from the film $s \in \{r, l\}$ is defined by the interfacial heat balance equation

$$h_{lv} \dot{m}_{fe,i}^{s,k} = U \pi d L_{f,i}^{s,k} [T_e - T_{sat}(P_i)]. \quad (3)$$

As discussed in the Introduction, the heat transfer coefficient is defined by the expression

$$U = \gamma \lambda_l / \delta_f, \quad (4)$$

where $\gamma \lesssim 1$ is a coefficient accounting for the spatial variation of the film thickness that exists in reality. The meaning of Eqs. (1, 2) is simple: the film length may decrease due to evaporation or due to the meniscus advancing in the direction of the film edge ("eating up" of the liquid film). The film length increases when the film is left during the receding motion of the meniscus (Landau-Levich film deposition). It is assumed that the triple contact line (i.e. film edge) is pinned and does not recede in the absence of evaporation.

The coordinates of the left and right film edges in each of $N_{e,i}$ evaporators ($X_{f,i}^{l,k}$ and $X_{f,i}^{r,k}$, respectively) may coincide with one of the ends of the evaporator or with a position of a meniscus if the corresponding film length is zero. Provided $X_i^l, X_i^r, L_{f,i}^{l,k}, L_{f,i}^{r,k}$ are known, $X_{f,i}^{l,k}$ and $X_{f,i}^{r,k}$ can be determined from the following reasoning.

When no part of the bubble situates in evaporators, $N_{e,i} = 1$ and the film is continuous as mentioned above. This is equivalent to a junction of the left and right films at a point (denoted X_j^1) that needs to be chosen. This choice is of importance because in the simulation it defines the point of the film rupture that may occur. Therefore $X_j^1 = X_{f,i}^{l,1} = X_{f,i}^{r,1}$ is assumed to coincide with the left or right meniscus (i.e with X_i^l or X_i^r), correspondingly to the direction of the bubble motion so that the evolution of the film edges exhibits no discontinuity when the Landau-Levich film begins to be deposed according to (1, 2).

When at least a part of the bubble situates in evaporators, one applies the following expressions to each of them ($k = 1 \ldots N_{e,i}$):

$$X_{f,i}^{l,k} = \left\{ \begin{array}{ll} X_i^l & \text{if } X_i^l \in k\text{-th evaporator} \\ X_{e,i}^{l,k} & \text{otherwise} \end{array} \right\} + L_{f,i}^{l,k}, \quad (5)$$

$$X_{f,i}^{r,k} = \left\{ \begin{array}{ll} X_i^r & \text{if } X_i^r \in k\text{-th evaporator} \\ X_{e,i}^{r,k} & \text{otherwise} \end{array} \right\} - L_{f,i}^{r,k}. \quad (6)$$

Here

$$X_{e,i}^{l,k} = L_p \left[\mathrm{int}\left(\frac{X_i^l - L_e}{L_p} \right) + k \right] \quad (7)$$

is the left edge of the k-th evaporator and $X_{e,i}^{r,k} = X_{e,i}^{l,k} + L_e$ is its right edge.

At some occasion, Eqs. (5, 6) may result in $X_{f,i}^{l,k} \geq X_{f,i}^{r,k}$ (i.e in a small film overlap allowed in the numerical calculation where the time steps are discrete). This signifies an appearance of a continuous liquid film. The point X_j^k (where the film will disrupt should the film rupture occur) needs to be defined. It is assumed to coincide with the point of film junction where the film is thinner there and likely to be evaporated quicker than elsewhere. Once X_j^k is defined, $X_{f,i}^{r,k}$ and $X_{f,i}^{l,k}$ are reassigned to X_j^k. Next, $L_{f,i}^{r,k}$ and $L_{f,i}^{l,k}$ are recalculated with Eqs. (5, 6).

2.2 Remaining vapor bubble governing equations

Condensation occurs to the film that surrounds a bubble portion $L_{c,i}$ located in the condenser. Similarly to the evaporation description, the film condensation rate $m_{fc,i}$ is defined by the expression

$$h_{lv} \dot{m}_{fc,i} = U \pi d L_{c,i} [T_{sat}(P_i) - T_c]. \quad (8)$$

Although much weaker than at the film interface, the mass exchange occurs at the remaining meniscus part (its portion of the size $L_m \ll d$ adjacent to the tube wall) and exists even if the film is evaporated completely. The heat

balance on the meniscus depends on whether the meniscus $s \in \{r,l\}$ situates inside the evaporator or the condenser,

$$h_{lv}\dot{m}^s_{me,i} = U_m \pi d L^s_{me,i}[T_e - T_{sat}(P_i)], \quad (9)$$

$$h_{lv}\dot{m}^s_{mc,i} = U_m \pi d L^s_{mc,i}[T_{sat}(P_i) - T_c], \quad (10)$$

where $U_m < U$ and

$$L^s_{me,i} = \begin{cases} L_m \text{ if } X^s_i \in \text{ evaporator}, \\ 0 \quad \text{otherwise}, \end{cases} \quad (11)$$

$$L^s_{mc,i} = \begin{cases} L_m \text{ if } X^s_i \in \text{ condenser}, \\ 0 \quad \text{otherwise}, \end{cases} . \quad (12)$$

(13)

The total bubble mass change rate $\dot{m}_i$ can be expressed as

$$\dot{m}_i = \sum_{s=r,l} \left[\sum_{k=1}^{N_{e,i}} \dot{m}^{s,k}_{fe,i} + \dot{m}^s_{me,i} - \dot{m}^s_{mc,i} \right] - \dot{m}_{fc,i}. \quad (14)$$

The energy equation of the i-th bubble is [16, 23]

$$m_i c_{vv} \dot{T}_i = \dot{m}_i R_v T_i + Q^{sens}_i - P_i S(\dot{X}^r_i - \dot{X}^l_i), \quad (15)$$

where the sensible heat exchange with the dry evaporator walls is described by the expressions

$$Q^{sens}_i = U_v \pi d L^{sens}_i (T_e - T_i), \quad (16)$$

where $U_v = 2\lambda_v/d$ (it is assumed that the boundary layer in the vapor is the tube radius) and

$$L^{sens}_i = \sum_{k=1}^{N_{e,i}} (X^{r,k}_{f,i} - X^{l,k}_{f,i}). \quad (17)$$

The vapor equation of state is approximated with the ideal gas equation

$$P_i = \frac{m_i R_v T_i}{S(X^r_i - X^l_i)}. \quad (18)$$

Note that the ideal gas assumption is used [16, 23] while deriving (15).

2.3 Liquid plug governing equations

The i-th liquid plug, i.e. that to the right of the i-th bubble, has the mass

$$m_{l,i} = \rho_l S(X^l_{i+1} - X^r_i), \quad (19)$$

where the index $i+1$ denotes the bubble to the right of the i-th bubble. The velocity V_i of the plug's center of mass is

$$V_i = 0.5(\dot{X}^l_{i+1} + \dot{X}^r_i). \quad (20)$$

It obeys the momentum equation

$$\frac{d(V_i m_{l,i})}{dt} = (P_i - P_{i+1})S - F_i \operatorname{sign}(V_i) + G_i, \quad (21)$$

where G_i is the gravity term discussed below. The viscous friction force F_i is defined by the expression corresponding to the single phase friction [18]

$$F_i = \frac{1}{2} K d \rho_l \pi (X^l_{i+1} - X^r_i) V_i^2 \quad (22)$$

$$K = \begin{cases} 16 & Re < 1 \\ 16/Re & 1 \le Re < 1180 \\ 0.078 Re^{-0.25} & Re \ge 1180 \end{cases},$$

$$Re = |V_i| d/\nu. \quad (23)$$

As in the previous modelling approaches, an additional contribution of the bends to F_i is neglected.

The liquid is assumed to be incompressible. This implies that the liquid plug volume may vary because of only two reasons: (i) phase change at its menisci and (ii) liquid film deposition or, on the contrary, "eating up". The velocity of the plug ends relative to its center of mass is thus non-zero and is defined by the change in the plug volume. This condition leads to the following condition of liquid mass balance in the plug:

$$\dot{m}_{l,i} = \dot{m}^l_{me,i+1} - \dot{m}^l_{mc,i+1} + \dot{m}^r_{me,i} - \dot{m}^r_{mc,i} + \pi d \delta_f \rho_l$$
$$\left[\begin{cases} 0 \quad \text{if } X^l_{i+1} \in \text{ evaporator}, \dot{X}^l_{i+1} > 0, \text{ and } L^{l,1}_{f,i+1} = 0, \\ \dot{X}^l_{i+1} \text{ otherwise.} \end{cases} \right.$$
$$\left. - \begin{cases} 0 \quad \text{if } X^r_i \in \text{ evaporator}, \dot{X}^r_i < 0 \text{ and } L^{r,N_{e,i}}_{f,i} = 0, \\ \dot{X}^r_i \text{ otherwise,} \end{cases} \right] \quad (24)$$

The upper options in both braces correspond to the meniscus advancement over the dry evaporator, and the lower options, to the film deposition or "eating up". The equations for $\dot{X}^l_i, \dot{X}^r_i$ need to be obtained from (19, 20, 24). It is evident that $\dot{X}^l_{i+1} \approx \dot{X}^r_i \approx V_i$ within quite small terms of the order δ_f/d and ρ_v/ρ_l that describe the liquid volume variation. For this reason, V_i can be used in the conditional clauses of (24) instead of $\dot{X}^l_{i+1}, \dot{X}^r_i$. The set of equations (19, 20, 24) becomes linear and can be solved straightforwardly for $\dot{X}^l_i, \dot{X}^r_i$. We do not however write their explicit expressions here because they are cumbersome.

The liquid volume variation was neglected in previous works. It is introduced here to provide the conservation of the total fluid mass in the PHP. A small error that arises when the conservation is violated accumulates and may become important at large simulation times.

2.3.1 Gravity term

The gravity sign is constant along each PHP branch but alters between branches, see Fig. 1c. The default gravity direction coincides with the x axis direction within the branch number $n = 0$ that starts at $x = 0.5L_e$. The gravity sign corresponding to the branch number n is thus $(-1)^n$. The branch number at a given x is

$$n_b(x) = \mathrm{int}\left(\frac{x - 0.5L_e}{L_b}\right). \tag{25}$$

The branch numbers of the liquid plug left and right ends are therefore $n_i^l = n_b(X_i^r)$ and $n_i^r = n_b(X_{i+1}^l)$, respectively. The gravity force reads

$$G_i = \rho_l S g \Bigg\{ (-1)^{n_i^r} \left[\left(X_{i+1}^l - \frac{1}{2}L_e \right) \bmod L_b - \frac{1}{2}L_b \right] - (-1)^{n_i^l} \left[\left(X_i^r - \frac{1}{2}L_e \right) \bmod L_b - \frac{1}{2}L_b \right] \Bigg\}. \tag{26}$$

It is evident that for $n_i^l = n_i^r$ (i.e. when the entire plug belongs to one branch),

$$G_i = m_{l,i} g (-1)^{n_i^l}. \tag{27}$$

The inclination angle θ of the PHP with respect to the vertical direction can be simulated by replacing g by $g\sin\theta$. $\theta = \pi$ can be used to describe the opposite (condenser on the top) PHP position.

2.3.2 Heat diffusion in liquid

The temperature distribution in the liquid plug $T_{l,i} = T_{l,i}(x,t)$ where $x \in (X_i^r, X_{i+1}^l)$ is governed by the heat diffusion equation [16],

$$\frac{\partial T_{l,i}}{\partial t} = D\frac{\partial^2 T_{l,i}}{\partial x^2} + D\frac{4Nu}{d^2}(T_{wall} - T_{l,i}). \tag{28}$$

The last term accounts for the heat transfer with the tube wall [16]. The Nusselt number depends on the plug velocity and length. The expressions for Nu for different ranges of Re are taken from [24]. T_{wall} is T_e or T_c depending on where x situates. The last term is absent at all if x belongs to the adiabatic section.

The boundary conditions for eq. (28) are given at the menisci:

$$T_{l,i}(X_i^r) = T_{sat}(P_i), \tag{29}$$

$$T_{l,i}(X_{i+1}^l) = T_{sat}(P_{i+1}). \tag{30}$$

Note that all previous equations of the model are independent of T_l because T_e and T_c are imposed and independent of the heat load. Eq. (28) can thus be solved *after* the calculation of the PHP dynamics. In our numerical code it is however solved together with all other equations so that the boundary conditions where T_e and T_c depend on the heat load could be easily implemented in the future.

2.4 Heat exchange rates

The instantaneous sensible heat power taken by the i-th bubble-plug pair from the evaporator is calculated with the following expression:

$$Q_{e,i}^{sens} = 2\pi\lambda_l \int Nu(T_e - T_{l,i})\mathrm{d}x + Q_i^{sens}, \tag{31}$$

where the integration is performed over the portion of the liquid plug located in the evaporator. The heat power given to the condenser is calculated accordingly,

$$Q_{c,i}^{sens} = 2\pi\lambda_l \int Nu(T_{l,i} - T_c)\mathrm{d}x, \tag{32}$$

where the integration is performed over the portion of the liquid plug located in the condenser. The instantaneous latent heat power taken by the i-th bubble-plug pair from the evaporator is

$$Q_{e,i}^{lat} = h_{lv} \sum_{s=r,l} \sum_{k=1}^{N_{e,i}} \dot{m}_{fe,i}^{s,k}. \tag{33}$$

That given to condenser is

$$Q_{c,i}^{lat} = h_{lv} \dot{m}_{fc,i}. \tag{34}$$

The instantaneous heat power is a sum of the corresponding terms over all bubbles of the PHP,

$$Q_s^k = \sum_i^M Q_{s,i}^k, \tag{35}$$

where $k \in \{sens, lat\}$ and $s \in \{e, c\}$. The total heat power reads

$$Q_s = Q_s^{lat} + Q_s^{sens}. \tag{36}$$

In the stationary regime, the condition

$$\langle Q_c \rangle = \langle Q_e \rangle, \tag{37}$$

where the angle brackets mean time average should be valid for long enough averaging times: the amount of heat taken from the evaporator should be equal to that given to the condenser.

2.5 Bubble-plug events

There are several kinds of events that can change the bubble-plug morphology. They cause a change of the equations to be solved on the next time step. One of such events, the film junction, was described in sec. 2.1. It changed equations but conserved their number. In this section, we rather discuss the events that change the number of both differential equations and unknowns.

First, it is the vapor bubble recondensation. It occurs when a moving liquid plug overtakes another plug. The vapor pressure grows and fast condensation occurs. A bubble located between two plugs completely disappears and a new long plug forms. Its mass is a sum of the masses of the parent plugs and its velocity is determined from the momentum conservation. On the next time step, the number of bubble-plug pairs drops by one and the number of equations reduces accordingly.

Another event met very often is a change in the number of liquid films. Such an event occurs when a bubble penetrates into extra evaporator or, on the contrary, withdraws from it. $N_{e,i}$ number then changes which means that the number of differential equations (1,2) changes too.

Other yet non implemented events include the vapor bubble creation by boiling or the complete liquid plug evaporation.

3 Numerical implementation

The spatial integration of eq. (28) is performed at each time step and needs to be discussed first.

3.1 Spatial integration of the heat diffusion equation

The i-th plug is divided to $N_{l,i}+2$ finite elements Δx_i^k. All (except of two ending) elements are of the same length; two ending elements are half-length. The element length varies slightly from plug to plug to keep the total number of elements integer. The node points X_i^k are in the centers of the internal $N_{l,i}$ elements. The node temperatures are denoted $T_{l,i}^k$. The temperature values at $X_i^0 = X_i^r$ and $X_i^{N_{l,i}+1} = X_{i+1}^l$ are given by the boundary conditions (29), so that there are $N_{l,i}$ unknown temperatures per plug. The finite volume method [25] is used and eq. (28) is integrated over each element. This results in the following discrete analog of equation (28) written for $k = 1 \dots N_{l,i}$,

$$\left.\frac{\partial T_{l,i}}{\partial t}\right|^k = \frac{2D}{\Delta x_i^k}\left(\frac{T_{l,i}^{k+1}-T_{l,i}^k}{\Delta x_i^{k+1}+\Delta x_i^k}+\frac{T_{l,i}^k-T_{l,i}^{k-1}}{\Delta x_i^k+\Delta x_i^{k-1}}\right) + D\frac{4Nu}{d^2}\left(T_{wall}-T_{l,i}^k\right). \quad (38)$$

3.2 Data structure

The code is object oriented and is written with C++. All variables are dynamically allocated. The code can thus deal with a PHP with arbitrary PHP geometry and time varying number of plugs, bubbles, and liquid films. The code makes use of the Microsoft Foundation Class (MFC) library to take advantage of the serialization (saving and restoring to/from data files) of the objects of the unknown in advance size. Each vapor bubble or liquid plug is implemented as a C++ object and encapsulates a number of scalar and vector "member" variables proper to each of them. The i-th bubble scalar members include $T_i, m_i, P_i, X_i^l, X_i^r, N_{e,i}, Q_{c,i}^{lat}, Q_{e,i}^{lat}$, a unique bubble identification number, and a pointer to the neighboring (from the right) liquid plug. The pointer is simply a computer memory address where the target object is located. The pointer may have null value to indicate the plug absence, which is useful to simulate the last bubble in the unlooped PHP. In the present article, only the closed loop PHP is considered so that each bubble has a plug. The vector member variables of the bubble include the liquid film lengths and edge coordinates. They are allocated dynamically and so that their length $N_{e,i}$ may vary. The scalar plug variables include $V_i, m_{l,i}, N_{l,i}, Q_{c,i}^{sens}, Q_{e,i}^{sens}$, and a pointer to its (left neighbor) bubble. The vector members of a plug are $\vec{\Delta x}_i$, $\vec{X}_i$, and $\vec{T}_{l,i}$.

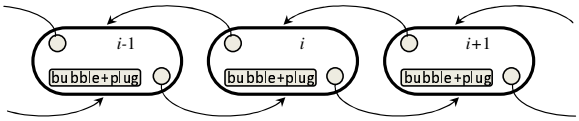

Fig. 3. Computer representation of the instantaneous state of the PHP as a doubly connected list. Each its node (an oval) contains the state of a bubble-plug pair and two pointers (circles) to the previous and to the next nodes.

In the remaining part of this section, the term PHP is used to denote the instantaneous state of all its bubbles and plugs. PHP is implemented as a doubly connected list (Fig. 3). The doubly connected list is an array, the i-th node of which contains the data (of a bubble and its plug) and the pointers to both previous and next nodes. Note that in this case i is an identifier of the node rather than its sequential number. The previous and the next nodes are denoted as $i-1$ and $i+1$ respectively just for the sake of illustration. The double connectivity allows fast access to these variables. Unlike the conventional (e.g. FORTRAN) arrays, such data structures can contain objects of different and variable length. This is convenient for several reasons. One of them is that the objects corresponding to plugs may contain the vectors of different and time-variable sizes $N_{l,i}$. The lists are convenient for another reason. Unlike the standard arrays, the list nodes are not necessarily written continuously into the computer memory. Therefore, it is very easy to suppress or, on the contrary, add a node somewhere in the middle of the PHP (which corresponds to the bubble recondensation or nucleation, respectively) without modifying the whole PHP in the computer memory. It is easy to understand from Fig. 3. Consider the suppression of the i-th node. It consists in redirection of the upper in Fig. 3 pointer of the node $i+1$ to the node $i-1$ and of the lower pointer of the node $i-1$ to the node $i+1$. The variables of the plug $i-1$ are changed to account for the plug coalescence as described in sec. 2.5 and

their numerical meshes used for liquid temperature calculation are merged. The i-th node can then be deallocated (i.e. the memory occupied by it is liberated). These changes do not concern other nodes so they are not modified at all. The standard array implementation would require the change of indices and a complete rewriting of the whole PHP into the computer memory, which would slow down the execution because the corresponding amount of information is quite large. For the closed loop PHP, the list is looped, i.e. a pointer belonging to the last node points to the first node and vice-versa.

The PHP states at different time moments are recorded as another list. As previously, the standard array cannot be used because the memory amount required for each PHP state may be different and is unknown in advance. This "PHP list" needs to be only simply connected, which means that each node contains the PHP and a (single) pointer to the next node. This pointer allows the sequential access to the PHP states, e.g. for plotting. The PHP list may also be saved to a data file of a specific `.php` format that can than be read by the postprocessing utility described below.

3.3 General algorithm

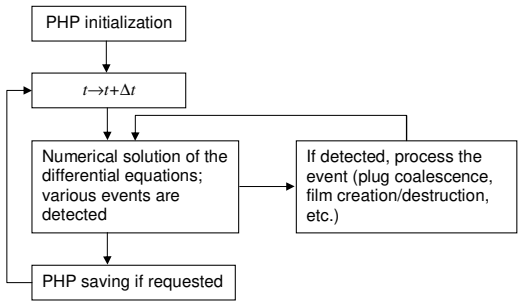

Fig. 4. General scheme of the C++ program.

The set of ordinary differential equations consists of eqs. (1, 2, 14, 15, 21, 24, 20, 38), which totals to $\sum_i^M (2N_{e,i} + N_{l,i} + 5)$ equations. Unlike previous works [16, 17, 22], they are written in the conventional differential form so that their numerical integration can be performed with any numerical method (and not only explicit Euler method used in [16, 17, 22]). The 4th order Runge-Kutta method (Fig. 4) is used here. It is renowned for its numerical stability and is thus better than the explicit method that can cause oscillations of numerical origin. The evaluation of the right-hand sides of the equations may lead to a detection of an event that changes the number of equations (see sec. 2.5). If detected, the event is processed as discussed in sec. 3.2. The number of equations and the equations themselves are updated and the time step is recalculated.

3.4 Data postprocessing

The number of PHP variables is large and changes in time. The data analysis is impossible without clear understanding of the position of each meniscus and film edge with respect to the PHP sections at each time moment. In the absence of a suitable commercial software, a specific data postprocessing "PHP_Viewer" utility had to be developed. PHP_Viewer possesses a conventional Microsoft Windows graphic user interface (Fig. 5). The name of the `.php` file is displayed close to the application name at the top of the screen above the menu. Some auxiliary information (the sequential number of the PHP record and the corresponding time) is shown in the status bar at the bottom of the screen. The evaporator (left) and condenser (right) locations are represented with rectangles, the width of which is to scale with respect to the PHP (see Fig. 1). The condenser and evaporator temperatures are displayed above them. The time of the current record is shown in between. The topology of the PHP bends is shown schematically with black connectors. The tube diameter is not to scale. The liquid temperature in the plugs is represented with a color. There are menu items usual for any video player. They allow controlling the animation speed and the navigation inside the data file (stepping record by record, jumping to a record with a given number, etc.).

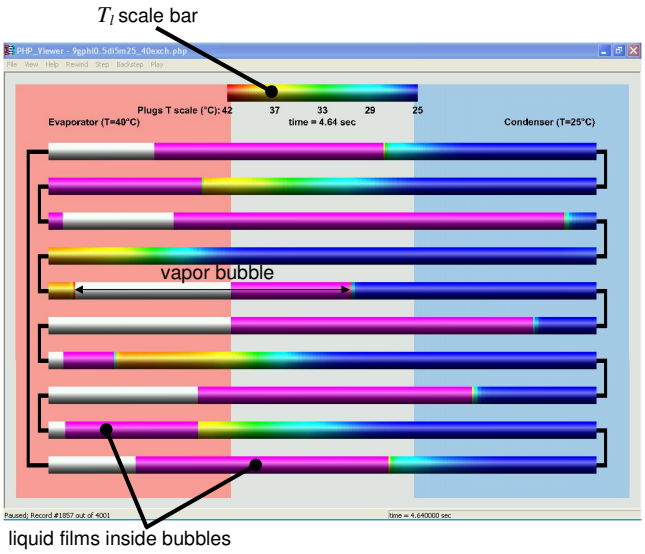

Fig. 5. (Color online) The screen of the PHP_Viewer version 1.6 in the liquid temperature visualization mode. The liquid films partially cover the internal tube walls inside the vapor bubbles. The temperature is indicated with coloring of the liquid plugs.

4 Results and discussion

The simulation runs were performed for the numerical parameters shown in Tab. 1. The initial temperature of the fluid was chosen to be homogeneous and equal to $0.5(T_e + T_c)$. The equidistant bubbles are distributed along the PHP. The menisci are initially at rest.

It is well known [6] that there are many different regimes of PHP functioning. The present modelling shows some of

PHP parameters	
Fluid	water
N_p	5
d	5 mm
L_e	10 cm
L_c	10 cm
L_a	5 cm

Constants	
γ	0.47
L_m	0.2 mm
U_m/U	0.3
Δt	10^{-4} s

Table 1. Parameters used for the numerical simulation.

them, in particular the regime of chaotic oscillations (Fig. 6). Its early stage is illustrated in Fig. 6a. Since the number of bubbles can only be reduced during the PHP evolution, their large number (usually 9) is chosen initially. Fig. 6a shows that the positions of some menisci join each other at $t < 0.2$ s. This corresponds to the bubble recondensation that occurs inside the condenser. The bubbles keep disappearing until only one per evaporator remains. The liquid gathers in the condenser under the action of gravity (cf. Fig. 1a). The film that remains in the evaporator does not, however, evaporate instantly (see the upper dotted line in Fig. 6a). This may cause an instability of the system, i.e. the development of oscillations. Their amplitude grows during a short transient before attaining the developed oscillation regime. The amplitude in this regime depends on the parameters (see below) and may be large. During large oscillations, the menisci penetrate both into the condenser and the evaporator. The films persist in the evaporator; the film length oscillates (see the dotted lines). The liquid volume change is almost invisible so that both ends of each liquid plug oscillate synchronously. A portion of the x axis corresponding to three plugs is shown in Fig. 6. They seem to oscillate quite independently. Even the amplitude of their oscillations may be different: compare the lower and upper plugs in Fig. 6b. The long-time PHP evolution (Fig. 6b) shows that the oscillations are indeed chaotic: no periodic repetition can be mentioned. This is a dynamic chaos well known to occur in the complex systems.

The regimes of oscillations are convenient to be presented at the heat transfer curve (Fig. 7). The oscillation exist when the temperature difference $\Delta T = T_e - T_c$ falls within an certain interval. Within this interval, one may distinguish the chaotic regime discussed above and the intermittent regime. The latter is characterized by a sequence of intervals during which the system oscillates strongly and the periods of weak motion. Generally the amplitude is very small near the lower oscillation threshold. Below the threshold, the oscillations decline to an equilibrium state where the vapor exists only in the evaporator and adiabatic sections and the condenser sections are completely filled by the liquid. The pressure inside the bubbles becomes equal to the saturation pressure corresponding to T_e, i.e. $T_e = T_{sat}(P_i)$ for every i. This state is attained via condensation/evaporation, during which the mass of the vapor in each bubble relaxes to that required by the vapor equation of state. The films in evaporator may exist but their lengths do not vary any more (cf. Eq. (3), the r.h.s. of which vanishes). At lower volume fractions, the liquid plugs do not fill completely the condenser sections so that the above equilibrium state cannot be attained: the heat exchange always exists. The stability of such a configuration is yet to be studied.

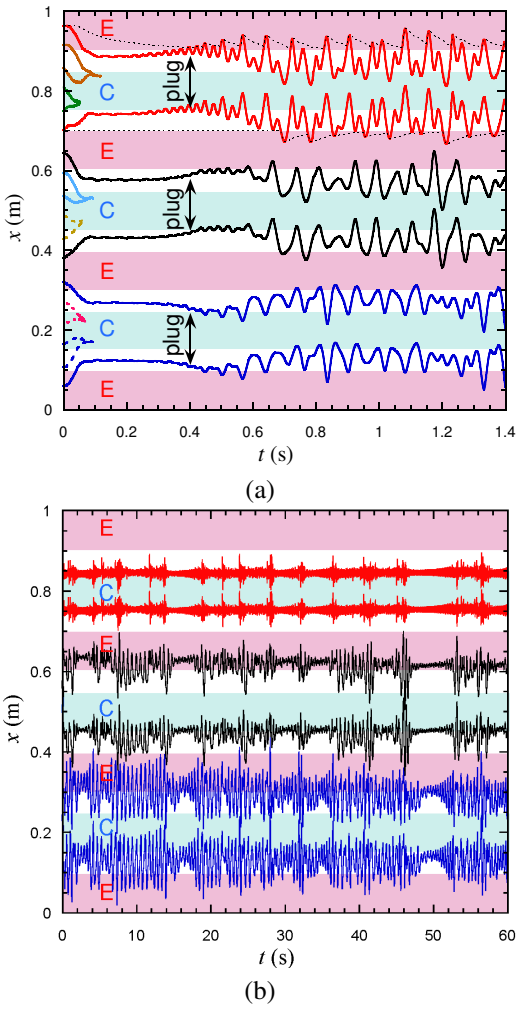

Fig. 6. (Color online) Examples of the chaotic oscillation regime within the linear PHP representation schematized in Fig. 1c. Evaporator (E) and condenser (C) sections are shown with the background bars; adiabatic sections are in between. PHP is shown partially with evolution of only several menisci. (a) Short time evolution. The bubble recondensation occurs at an early stage. The evolution of only two film edges is shown by dotted lines. (b) Long time evolution for $T_e = 45^\circ$ C, $T_c = 25^\circ$ C, $\phi = 0.55$, $\delta_f = 40\,\mu$m.

When ΔT is larger than the upper oscillation threshold, the initial perturbation eventually declines. However the scenario is different from the low ΔT case. During the initial transient, the oscillations develop. Their amplitude becomes large like in the chaotic regime; the bubbles are compressed strongly between the plugs which have different inertia and thus move with different velocities. At some point one of the bubbles is compressed so strongly that it recondenses. This leads to a creation of a liquid plug with yet larger inertia, which causes the bubble recondensation in chain that in

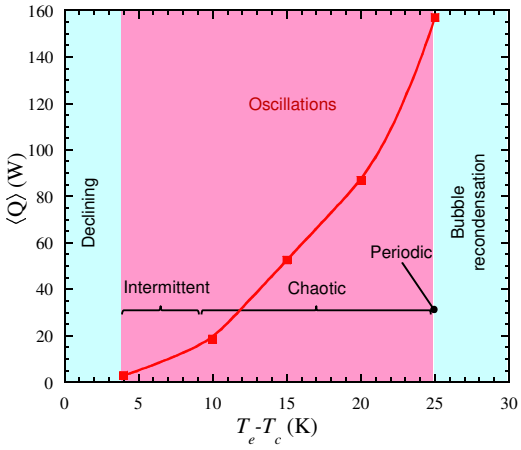

Fig. 7. (Color online) Heat transfer curve and PHP regimes for $T_c = 25^\circ$ C, $\phi = 0.55$, $\delta_f = 40\ \mu$m.

most cases ends up in a creation of a single plug and a single bubble and the motion stops.

It is likely that the introduction of boiling will cause an instability of the final equilibrium state of the bubble recondensation regime. Indeed, in the final single bubble state the liquid situates necessarily in the evaporator and the boiling should occur and cause a restart of the oscillations.

The oscillation regime depends strongly on the chosen value of the film thickness δ_f. The influence of δ_f was studied for the following set of the fixed parameters: $T_e = 35^\circ$ C, $T_c = 25^\circ$ C, $\phi = 0.55$. It turns out that the δ_f decrease leads to the same sequence of regimes as ΔT growth. At $\delta_f > 90\ \mu$m the self sustained oscillations are nonexistent. The δ_f decrease leads to an appearance of the intermittent oscillations. Their amplitude grows as δ_f decreases until the bubble recondensation appears and causes the oscillation disruption at $\delta_f \approx 5\ \mu$m. This shows the importance of the δ_f choice.

The heat transfer rate varies chaotically (Fig. 8a) during the oscillations accordingly to the dynamics of the menisci. During the developed oscillations, the equality (37) is satisfied within few per cent. The sensible heat exchange part may however be different in the condenser and in the evaporator (Fig. 8b). It is comprehensible since the condenser is occupied by the liquid most of the time. Accordingly, a part of the sensible heat exchange in the condenser is larger than in the evaporator. The part of the sensible heat exchange increases with the amplitude of the oscillations because the liquid sweeps more often hot and cold walls. The averaged in time Q value is shown in Fig. 7 as a function of ΔT. One can see that quite efficient heat exchange can be achieved even without boiling that is likely to lead to the continuation of the curve into the "bubble recondensation" region as discussed above.

The temperature inside the liquid is inhomogeneous, see Fig. 5b. One can see the thermal boundary layers that form near the menisci inside the liquid plugs. They appear because the pressure (and thus the gas-liquid interface temperature T_{sat}) changes quickly during the oscillations; T_{sat} is sometimes 40-50 K larger than T_e. The analysis shows that the

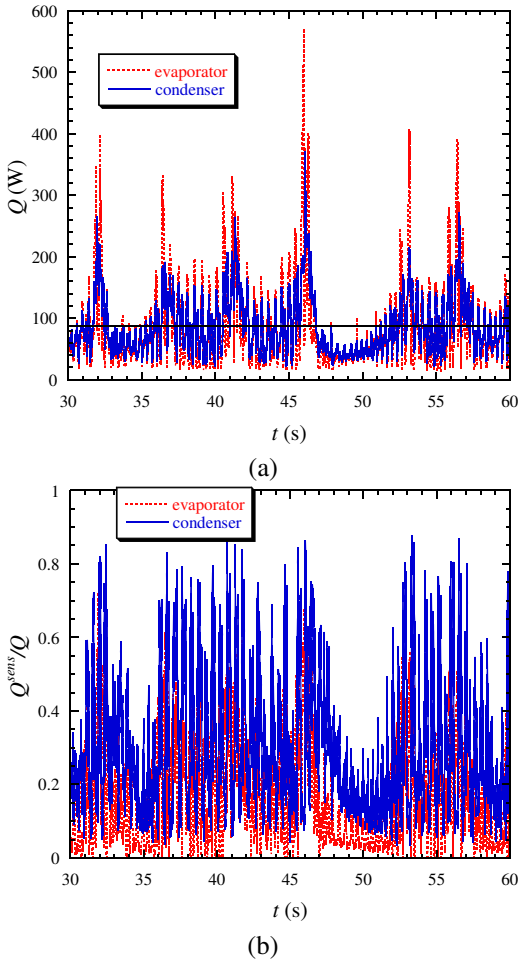

Fig. 8. (Color online) Examples of the PHP heat exchange rate evolution in condenser and evaporator for the same parameters as Fig. 6b. (a) Total heat exchange. The time average $\langle Q \rangle$ is shown with a horizontal line. (b) Part of the sensible heat exchange. The average values are 0.18 for evaporator and 0.29 for condenser.

vapor pressures can also attain high values. The vapor temperature rises strongly due to this compression and can be essentially higher than T_e (Fig. 9). This has been already observed in the single-bubble modelling [15]. During the developed oscillations, the vapor is overheated: its temperature exceeds T_{sat} by 10-20 K on average. This shows that the hypothesis [20, 21] about the vapor at saturation temperature is hardly consistent.

The thickness of the boundary layers is different in different liquid plugs. It is defined by the value $\sqrt{D\tau}$ where τ is an average period of the oscillations of a plug that grows with its mass.

5 Conclusions

A new model for PHP with arbitrary number of branches and arbitrary time-varying number of bubbles has been presented above. It is more complex than the previous models and is capable of describing the chaotic self-sustained oscillations of large amplitude. It is shown to reproduce correctly some features of experimental models like intermittent oscil-

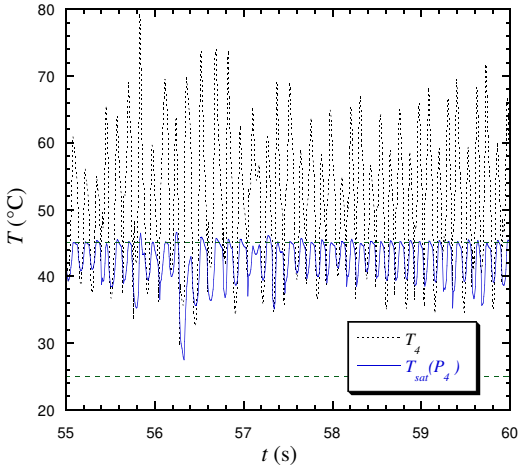

Fig. 9. (Color online) Typical evolution of temperatures obtained for a bubble from Fig. 6b. The evolution of the left and right ends of this bubble correspond to the third and the second curves from the top of Fig. 6b, respectively. The horizontal dashed lines correspond to T_c and T_e.

lation regime. Some analysis of the flow in the PHP and the heat transfer has been performed. An oscillation threshold occurs at small temperature difference. Another threshold, that occurs at a large temperature difference would probably be yet larger if the boiling were taken into consideration. The boiling thus needs to be implemented.

More studies need to be performed even for the present formulation of the model. In particular, the influence of the initial conditions (initial values of M, T_i, X_i^s, etc.) might be of importance because the system is chaotic.

To perform more realistic modelling, more information is required on the phenomena that occur during the PHP functioning. In particular, it is a priori evident that a strong viscous dissipation occurs in the liquid films and near the contact lines (i.e. film edges). This effect leads to an additional pressure drop across each meniscus. The available in the literature information on this phenomenon is scarce. The effect of the PHP bends on the pressure drop should be accounted for. The film thickness is an important parameter, which was imposed here to be constant and is taken to be micrometric like in previous works [18, 19]. However it depends on the plug velocity and possibly on the evaporation/condensation rate and should thus vary with time. Third, the vapor compression has not been yet assessed experimentally. It is not clear if the liquid plug return force is caused entirely by the evaporation/condensation effect (assumed in the models where the vapor was always at saturation temperature) or also by the vapor compression like in the present approach.

Achnowledgements

Two of my students, B. Pottier and A. Tanniou, participated in the development of the simulation code during their four month internship in our laboratory. Their contribution is gratefully acknowledged as well as the corresponding CEA/SBT grants.

Nomenclature

c_{vv}	vapor specific heat at constant volume [J/(kg·K)]
D	liquid heat diffusivity [m^2/s]
d	tube diameter [m]
F	viscous friction force [N]
G	gravity force [N]
g	gravity acceleration [m^2/s]
h_{lv}	latent heat [J/kg]
K	friction coefficient
L	length [m]
M	total number of bubbles or plugs
m	mass (of vapor by default) [kg]
N	total number
n	sequential branch number
Nu	liquid Nusselt number
P	vapor pressure [Pa]
Q	heat exchange rate [W]
R_v	vapor gas constant [J/(kg·K)]
Re	liquid Reynolds number
S	tube section area [m^2]
T	temperature (T_i: of vapor) [K]
t	time [s]
U	heat transfer coefficient (of film transfer if no indices) [W/(K·m^2)]
V	velocity (V_i: of liquid plug) [m/s]
X	absolute position at the x axis [m]

Greek symbols

Δ	difference
δ_f	liquid film thickness [m]
γ	coefficient in Eq. 4
λ	heat conductivity [W/(m·K)]
ν	liquid kinematic viscosity [m^2/s]
ϕ	volume fraction of liquid in PHP
ρ	density [kg/m^3]

Superscripts

k	index
l	left
lat	latent
r	right
s	r or l
$sens$	sensible

Subscripts

a	adiabatic
b	branch
c	condenser
e	evaporator
f	liquid film
i	bubble or plug identifier
j	film junction
l	liquid
m	meniscus
p	PHP spatial period
s	e or c

sat	at saturation
t	total
v	vapor
wall	internal tube wall

References

[1] Akachi, H., 1993. Structure of micro-heat pipe. US Patent 5219020, 15 June.

[2] Vasiliev, L. L., 2005. "Heat pipes in modern heat exchangers". *Appl. Therm. Eng.,* **25**(1), pp. 1 – 19.

[3] Zhang, Y., and Faghri, A., 2008. "Advances and unsolved issues in pulsating heat pipes". *Heat Transfer Eng.,* **29**(1), pp. 20 – 44.

[4] Tong, B. Y., Wong, T. N., and Ooi, K. T., 2001. "Closed-loop pulsating heat pipe". *Appl. Therm. Eng.,* **21**(18), pp. 1845 – 1862.

[5] Miyazaki, Y., and Arikawa, M., 1999. "Oscillatory flow in the oscillating heat pipe". In Proc. 11th Int. Heat Pipe Conf., pp. 143 – 148.

[6] Khandekar, S., Charoensawan, P., Groll, M., and Terdtoon, P., 2003. "Closed loop pulsating heat pipes Part B: visualization and semi-empirical modeling". *Appl. Therm. Eng.,* **23**(16), pp. 2021 – 2033.

[7] Xu, J., Li, Y., and Wong, T., 2005. "High speed flow visualization of a closed loop pulsating heat pipe". *Int. J. Heat Mass Transfer,* **48**(16), pp. 3338 – 3351.

[8] Gi, K., Sato, F., and Maezawa, S., 1999. "High speed flow visualization of a closed loop pulsating heat pipe". In Proc. 11th Int. Heat Pipe Conf., pp. 149 – 153.

[9] Inoue, T., Kouduma, T., Senjaya, R., and Suzuki, Y., 2010. "Bubble generation in oscillating heat pipe". In Proc. 15th Int. Heat Pipe Conf., Clemson University.

[10] Charoensawan, P., Khandekar, S., Groll, M., and Terdtoon, P., 2003. "Closed loop pulsating heat pipes: Part A: parametric experimental investigations". *Appl. Therm. Eng.,* **23**(16), pp. 2009 – 2020.

[11] Li, J., and Yan, L., 2008. "Experimental research on heat transfer of pulsating heat pipe". *J. Therm. Sci.,* **17**(2), June, pp. 181 – 185.

[12] Ma, H. B., Borgmeyer, B., Cheng, P., and Zhang, Y., 2008. "Heat transport capability in an oscillating heat pipe". *J. Heat Transfer,* **130**(8), p. 081501.

[13] Maydanik, Y. F., Dmitrin, V. I., and Pastukhov, V. G., 2009. "Compact cooler for electronics on the basis of a pulsating heat pipe". *Appl. Therm. Eng.,* **29**(17-18), pp. 3511 – 3517.

[14] Lips, S., Bensalem, A., Bertin, Y., Ayel, V., Romestant, C., and Bonjour, J., 2010. "Experimental evidences of distinct heat transfer regimes in pulsating heat pipes (PHP)". *Appl. Therm. Eng.,* **30**(8-9), pp. 900 – 907.

[15] Das, S., Nikolayev, V., Lefèvre, F., Pottier, B., Khandekar, S., and Bonjour, J., 2010. "Thermally induced two-phase oscillating flow inside a capillary tube". *Int. J. Heat Mass Transfer,* **53**(19-20), pp. 3905 – 3913.

[16] Shafii, M. B., Faghri, A., and Zhang, Y., 2001. "Thermal modeling of unlooped and looped pulsating heat pipes". *J. Heat Transfer,* **123**(6), pp. 1159 – 1172.

[17] Sakulchangsatjatai, P., Terdtoon, P., Wongratanaphisan, T., Kamonpet, P., and Murakami, M., 2004. "Operation modeling of closed-end and closed-loop oscillating heat pipes at normal operating condition". *Appl. Therm. Eng.,* **24**(7), pp. 995 – 1008.

[18] Dobson, R. T., 2004. "Theoretical and experimental modelling of an open oscillatory heat pipe including gravity". *Int. J. Therm. Sci.,* **43**(2), pp. 113 – 119.

[19] Dobson, R. T., 2005. "An open oscillatory heat pipe water pump". *Appl. Therm. Eng.,* **25**(4), pp. 603 – 621.

[20] Zhang, Y., and Faghri, A., 2002. "Heat transfer in a pulsating heat pipe with open end". *Int. J. Heat Mass Transfer,* **45**(4), pp. 755 – 764.

[21] Holley, B., and Faghri, A., 2005. "Analysis of pulsating heat pipe with capillary wick and varying channel diameter". *Int. J. Heat Mass Transfer,* **48**(13), pp. 2635 – 2651.

[22] Senjaya, R., Inoue, T., and Suzuki, Y., 2010. "Oscillating heat pipe simulation with bubble generation". In Proc. 15th Int. Heat Pipe Conf., Clemson University.

[23] Nikolayev, V. S., 2011. "Comment on "Flow and heat transfer of liquid plug and neighboring vapor slugs in a pulsating heat pipe" by Yuan, Qu, & Ma". *Int. J. Heat Mass Transfer,* **54**(9-10), pp. 2226 – 2227.

[24] Bejan, A., 2004. *Convection Heat Transfer*, 3rd ed. Wiley, Hoboken.

[25] Patankar, S. V., 1980. *Numerical heat transfer and fluid flow*. Hemisphere, Washington.